

A Combined Experimental and Computational Study of the Substituent Effect on Micellar Behavior of γ -Substituted Thermoresponsive Amphiphilic Poly(ϵ -caprolactone)s

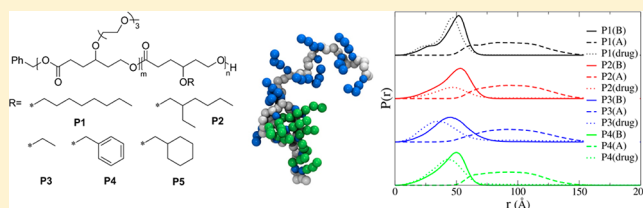
Jing Hao,^{‡,§} Yixing Cheng,^{†,§} R. J. K. Udayana Ranatunga,[‡] Suchithra Senevirathne,[‡] Michael C. Biewer,[‡] Steven O. Nielsen,[‡] Qian Wang,[†] and Mihaela C. Stefan^{*,‡}

[†]Department of Chemistry and Biochemistry, University of South Carolina, Columbia, South Carolina 29208, United States

[‡]Department of Chemistry, University of Texas at Dallas, Richardson, Texas 75080, United States

Supporting Information

ABSTRACT: The effect of the core substituent structure on the micellar behavior of thermoresponsive amphiphilic poly(ϵ -caprolactone) diblock copolymer micelles was investigated through a combination of experimental and computational methods. The polycaprolactone (PCL) amphiphilic block copolymers used in this study consisted of a hydrophilic poly{ γ -2-[2-(2-methoxyethoxy)ethoxy]ethoxy- ϵ -caprolactone} block, which also endowed the polymer with thermoresponsiveness, and various hydrophobic poly(γ -alkoxy- ϵ -caprolactone) blocks. Five different substituents have been attached to the γ -position of the ϵ -caprolactone of the hydrophobic block, namely octyloxy, ethylhexyloxy, ethoxy, benzyloxy, and cyclohexylmethoxy, which self-assembled in aqueous media to generate the core of the micelles. All five synthesized diblock copolymers formed micelles in water and displayed thermoresponsive behavior with lower critical solution temperature (LCST) in the range of 36–39 °C. The impact of different substituents on the micelle properties such as size, stability, and phase transition behavior was investigated. Drug loading and release properties were also studied by employing doxorubicin (DOX) as payload. Molecular dynamics modeling was used to predict the variation of particle size, free volume, and drug loading capacity. The drug loading capacity predicted from molecular dynamics simulation was found to be comparable with the experimental data, which suggests that molecular dynamic simulation may be a useful tool to provide valuable selection criteria for the engineering of polymeric micelles with tunable size and drug loading capacity.



INTRODUCTION

Polymeric micelles are core–shell structures formed by self-assembly of amphiphilic block copolymers.^{1–5} The hydrophobic core acts as a microreservoir for the encapsulation of drugs, while the hydrophilic shell acts as a corona which protects the micelles from protein adsorption and cellular adhesion. Among the polymeric micelle systems under clinical study, micelles formed from amphiphilic aliphatic polyesters have shown great promise due to their superior biocompatibility and biodegradability. Moreover, due to the flexibility and feasibility of chemical modification of polyesters,^{6–8} the properties of these micelles can be tailored by introducing functional groups to the core or shell to optimize delivery efficacy and maximize the therapeutic effect.⁹ For instance, micellar cores have been conjugated with functional groups, drug molecules, or cross-linked to enhance drug loading capacity, micelle stability, and controlled release properties.^{10–13} Moreover, micellar shells have been engineered to achieve active targeting, enhanced cellular uptake, and stimuli-responsive drug release properties.^{14–17}

Imparting thermoresponsive properties to the micelles allows the micelle to release encapsulated molecules in a controlled manner upon temperature change.^{18–20} Oligo(ethylene glycol)

(OEG) polymers have emerged as a new class of thermoresponsive polymers.^{21,22} The phase transition behavior of the OEG-functionalized polymers have been shown to be insensitive to ionic strength, concentration, etc., and thus are superior to N-substituted acrylamide polymers, like PNIPAM.²¹ In addition, polymeric micelles from OEG grafted polymers have shown controllable drug release and improved cellular uptake in response to temperature increase.²³ In our previous studies, we have reported the synthesis of tri(ethylene glycol)-substituted amphiphilic polycaprolactone diblock copolymer (PMEEEL-*b*-POCTCL) and its self-assembled micelle.¹⁴ The drug loading, cytotoxicity, and thermo-induced drug release behavior of this polymeric micelle system have also been studied.²⁴ The obtained experimental results indicated that this polyester-based amphiphilic diblock copolymer is an ideal polymeric micelle system for controlled drug release, thus deserving further investigation.

Micelle core engineering represents a promising methodology to optimize various properties of a micelle as a drug

Received: April 25, 2013

Revised: May 30, 2013

vector.⁹ Rationally designed functionalities of the micelle core are expected to enhance the overall performance of micelle nanocarriers by tuning the drug loading capacity, stability, and “smartness”.^{10–12,25,26} Previously, we employed an octyloxy substituent attached to the γ -position of the ϵ -caprolactone to form the micelle core. However, only moderate drug loading and stability were achieved. To further optimize this class of amphiphilic thermoresponsive polycaprolactone block copolymers as drug carriers and systematically study the substituent effect on the micellar assembly, we synthesized five polycaprolactone amphiphilic block copolymers with different hydrophobic substituents. Octyloxy, ethylhexyloxy, ethoxy, benzylloxy, and cyclohexylmethoxy were used as substituents on the core-forming block. The substituents were chosen to compare linear vs branched aliphatic substituents, long vs short aliphatic substituents, and aromatic vs nonaromatic ring substituents. These functionalities on the core segment were expected to interact intra- and intermolecularly with the encapsulated drug molecules by noncovalent interactions, such as hydrophobic, π - π stacking, and hydrogen bonding. Doxorubicin (DOX) was employed as a model drug as its interactions with polymer chains govern the encapsulation behavior by polymeric micelles.¹² In summary, the substituent effect on thermal-induced phase transition, thermodynamic and kinetic stability, drug loading, and thermo-induced drug release of DOX were investigated for this library of polycaprolactone amphiphilic block copolymers.

In addition to exploring the substituent effect experimentally, we were also interested in whether the micellar behavior can be predicted by molecular dynamics (MD) simulation. While molecular dynamics has been applied to study micellation behavior,^{27,28} this is the first report of using MD methodology to study the substituent effect of polymeric micelles. MD simulations were performed for micelles with the same polymer backbone and similar functional hydrophobic substituents as the experimentally synthesized polymers. The drug loading behavior was predicted by using phenol as a DOX alternative. The free volume of the micellar core was calculated for both drug loaded and unloaded micelles. The results indicated that the interaction between the drug and polymer is more important than the void volume of the micelle cores in determining the drug loading capacity (DLC).

MATERIALS AND METHODS

Materials and Characterization. All commercial chemicals were purchased from Aldrich Chemical Co., Inc., and were used without further purification unless otherwise noted. Stannous(II) 2-ethylhexanoate was purified by vacuum distillation prior to use. γ -Octyloxy- ϵ -caprolactone and γ -2-[2-(2-methoxyethoxy)ethoxy]ethoxy- ϵ -caprolactone monomers were synthesized according to the previously reported procedure.¹⁴

¹H NMR spectra of the synthesized monomers and polymers were recorded on a Bruker 500 MHz spectrometer at 30 °C in CDCl₃. ¹H NMR data are reported in parts per million as chemical shift relative to tetramethylsilane (TMS) as the internal standard. GC/MS was performed on an Agilent 6890-5973 GC-MS workstation. The following conditions were used for all GC/MS analyses: injector and detector temperature, 250 °C; initial temperature, 70 °C; temperature ramp, 10 °C/min; final temperature, 280 °C. Molecular weights of the synthesized polymers were measured by size exclusion chromatography (SEC) analysis on a Viscotek VE 3580 system equipped with Viscogel columns (GMHHR-M), connected to a refractive index (RI) detector. GPC solvent/sample module (GPCmax) was used with HPLC grade THF as the eluent, and calibration was based on polystyrene standards. Running conditions for SEC analysis were flow

rate = 1.0 mL/min, injector volume = 100 μ L, detector temperature = 30 °C, and column temperature = 35 °C. All the polymers samples were dissolved in THF, and the solutions were filtered through PTFE filters (0.45 μ m) prior to injection.

General Procedure for the Synthesis of Amphiphilic Diblock Copolymers P1–P5. All the monomers were dried by azeotropic distillation from toluene before the reaction. Dried γ -2-[2-(2-methoxyethoxy)ethoxy]ethoxy- ϵ -caprolactone (0.5 g, 1.8×10^{-3} mol) was transferred into a flame-dried 10 mL Schlenk flask under a nitrogen atmosphere. Stock solutions of Sn(Oct)₂ (0.016 g, 3.6×10^{-5} mol) in hexane and benzyl alcohol (0.004 g, 3.6×10^{-5} mol) in hexane were added to the Schlenk flask under a nitrogen atmosphere. The reaction mixture was deoxygenated by three consecutive freeze–pump–thaw cycles, and the vacuum of the last cycle was canceled with nitrogen. The reaction flask was heated in a thermostated oil bath at 110 °C for 4 h. At this time a sample was collected to determine the monomer conversion and molecular weight by ¹H NMR analysis. Deoxygenated monomers (M1–M5) (1.8×10^{-3} mol) were added to the reaction flask under a nitrogen atmosphere, and the reaction was left overnight at 110 °C.

Poly{ γ -2-[2-(2-methoxyethoxy)ethoxy]ethoxy- ϵ -caprolactone}-*b*-poly(γ -octyloxy- ϵ -caprolactone) (P1). ¹H NMR (500 MHz, CDCl₃): δ_{H} 0.89 (t, 3H), 1.27 (m, 10H), 1.54 (m, 2H), 1.80 (m, 8H), 2.38 (m, 4H), 3.38 (m, 6H), 3.60 (m, 13H), 4.15 (m, 4H) (the polymer contains 53.5% PMEEE).

Poly{ γ -2-[2-(2-methoxyethoxy)ethoxy]ethoxy- ϵ -caprolactone}-*b*-poly(γ -2-ethylhexyloxy- ϵ -caprolactone) (P2). ¹H NMR (500 MHz, CDCl₃): δ_{H} 0.87 (m, 6H), 1.27 (m, 9H), 1.80 (m, 8H), 2.37 (m, 4H), 3.38 (m, 3H), 3.60 (m, 16H), 4.16 (b, 4H) (the polymer contains 54.1% PMEEE).

Poly{ γ -2-[2-(2-methoxyethoxy)ethoxy]ethoxy- ϵ -caprolactone}-*b*-poly(γ -ethoxy- ϵ -caprolactone) (P3). ¹H NMR (500 MHz, CDCl₃): δ_{H} 1.17 (t, 3H), 1.8 (m, 8H), 2.39 (m, 4H), 3.38 (s, 3H), 3.47 (m, 3H), 3.59 (m, 13H), 4.17 (t, 4H) (the polymer contains 62.8% PMEEE).

Poly{ γ -2-[2-(2-methoxyethoxy)ethoxy]ethoxy- ϵ -caprolactone}-*b*-poly(γ -benzylloxy- ϵ -caprolactone) (P4). ¹H NMR (500 MHz, CDCl₃): δ_{H} 1.80 (m, 8H), 2.37 (m, 4H), 3.38 (s, 3H), 3.59 (m, 14H), 4.15 (b, 4H), 4.47 (m, 2H), 7.30 (b, 5H) (the polymer contains 54.4% PMEEE).

Poly{ γ -2-[2-(2-methoxyethoxy)ethoxy]ethoxy- ϵ -caprolactone}-*b*-poly(γ -cyclohexylmethoxy- ϵ -caprolactone) (P5). ¹H NMR (500 MHz, CDCl₃): δ_{H} 0.93 (m, 2H), 1.24 (m, 3H), 1.81 (m, 14H), 2.40 (m, 4H), 3.22 (m, 2H), 3.40 (s, 3H), 3.62 (m, 14H), 4.18 (m, 4H) (the polymer contains 53.4% PMEEE).

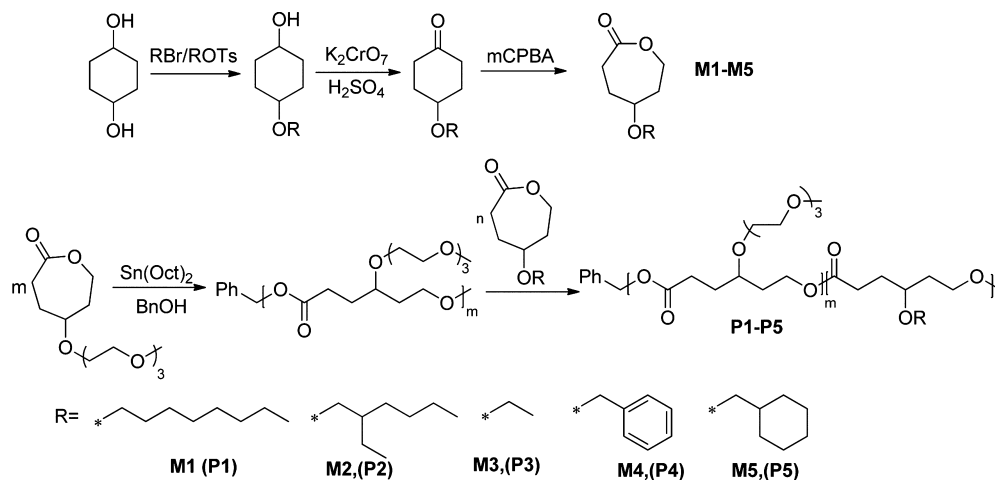
Preparation of Polymeric Micelles and Drug Encapsulation.

Each polymer (20 mg) was dissolved in 1 mL of THF, and 40 μ L of the polymer THF solution was added dropwise to 4 mL of deionized water under vigorous agitation. THF was removed by dialyzing the mixture against deionized water for 1 day (MWCO = 3 kDa). The micelle suspension was filtered through a 0.45 μ m filter before characterization. Doxorubicin (DOX) was encapsulated in polymeric micelles as a model hydrophobic guest molecule. DOX was first treated with 3 equiv of triethylamine in DMSO. The neutralized DOX solution was mixed with each polymer THF solution at a mass ratio of 1:10. The polymer/DOX mixture (40 μ L) was added dropwise to 4 mL of deionized water under vigorous agitation. The DOX-loaded micelle suspension was dialyzed against deionized water for 1 day and then filtered with a 0.45 μ m filter before characterization. Equivalent DOX concentration in the micelles was determined by fitting readout absorbance of DOX loaded micelles at 485 nm to a pre-established standard curve of DOX. Loading efficiency (LE) and loading capacity (LC) of all polymeric micelles, assuming there was no loss of polymer during sample preparation, were calculated according to the following equations:

$$\text{LE (wt \%)} = \frac{\text{weight of encapsulated DOX}}{\text{weight of total DOX}} \times 100\%$$

$$\text{LC (wt \%)} = \frac{\text{weight of encapsulated DOX}}{\text{weight of polymer}} \times 100\%$$

Scheme 1. Synthesis of Monomers (M1–M5) and Diblock Copolymers (P1–P5)



$$\text{LC (mol \%)} = \frac{\text{weight of encapsulated DOX/MW of DOX}}{\text{weight of polymer}/(\text{DP} \times \text{mass of repeating unit})} \times 100\%$$

Micelle Characterization. Particle size, size distribution, and zeta potential of blank and DOX-loaded micelles were studied by dynamic light scattering (DLS) performed on a Zetasizer Nano ZS (Malvern Instrument) using the filtered suspension without further dilution. All measurements were carried out at 25 °C. Optical transmittance of polymeric micelles in response to temperature change was monitored. Briefly, a polymeric micelle (2–4 mg/mL) suspension was subjected to gradual heating followed by transmittance measurement by UV–vis at 600 nm. The lower critical solution temperature (LCST) of the micelle solution was defined as the temperature at which the transmittance decreased to 50% of its original value. The critical micellar concentration (CMC) was determined by fluorescence spectroscopy using pyrene as a fluorescent probe. Pyrene loaded micelles were prepared at various polymer concentrations ($0.1\text{--}10^{-4}$ g/L) while the pyrene concentration was kept constant at 3.3×10^{-6} M. Fluorescence excitation spectra (emission at 390 nm) were recorded on a FP-6200 spectrofluorometer. The morphology of blank and DOX-loaded micelles was investigated by transmission electron microscopy (TEM, Hitachi H-8000). TEM samples were prepared by dipping the micelle suspension onto the grid. Extra suspension was blotted by Kimwipe. After air-drying, the sample grid was stained with 2% uranyl acetate and viewed at 200 kV accelerating voltage.

In Vitro Kinetic Stability. The *in vitro* kinetic stability of micelles composed of various polymers was measured using Förster resonance energy transfer (FRET)-based technology.²⁹ To prepare FRET micelles, the FRET pair 1,1'-dioctadecyl-3,3,3',3'-tetramethylindocarbocyanine perchlorate (DiI), 3,3'-dioctadecyloxycarbocyanine perchlorate (DiO) was mixed with the polymer (1:100, w/w), and the mixture was used to prepare FRET micelles using the aforementioned procedure. The FRET micelle suspension were suspended in 30% FBS. The micelle suspension was placed on an orbital shaker at room temperature. At predesigned time intervals, the fluorescence spectra of all FRET micelles were recorded using a fluorospectrometer. The excitation was 484 nm, which is the excitation maximum of DiO. Emission spectra were collected from 490 to 600 nm. The kinetic stability of the micelles was quantified by the FRET ratio $I_{565}/(I_{501} + I_{565})$. I_{501} and I_{565} are the fluorescence intensity at 501 and 565 nm, respectively.

In Vitro Drug Release. Nile Red was chosen as a model hydrophobic guest to study the substituent effect on the thermo-induced release behavior of various polymeric micelles. Nile Red (1:10, w/w) containing micelles were prepared in PBS using a similar procedure as previously described.²⁴ The Nile Red loaded micelles were either incubated at room temperature or at 43 °C, which is higher than the LCST of all polymers as previously determined. The time-

resolved fluorescence spectra of Nile Red loaded micelles were recorded on a fluorospectrometer at predetermined time intervals (excitation at 570 nm). The release percentage was represented by the normalization of fluorescence intensity at 620 nm to the fluorescence intensity of time zero.

Molecular Dynamics Simulations. The SDK coarse-grained (CG) force field was used for molecular dynamics computer simulations.^{30–32} This force field incorporates 3–4 heavy atoms and their associated hydrogen atoms into a single CG bead. This representation is used to achieve time and length scales necessary to simulate aqueous polymer micelles. Simulations were carried out using the LAMMPS code maintained by Sandia National Laboratories.³³ Simulations were run using a multistep rRESPA integrator,³³ where an outer time step of 10 fs was used for the nonbonded interactions and a time step of 2.5 fs was used for the bonded interactions. A Nose–Hoover thermostat (at 300 K) and barostat (at 1 atm)³⁴ were used to generate system configurations from the isothermal–isobaric (NPT) ensemble.

Simulation of Micelles. Initial coordinates for monomer units were created by hand and repeated as required to obtain single polymer chains consisting of a polycaprolactone backbone with 20 hydrophilic and hydrophobic pendant groups. Simulations were carried out on polymer chains that have similar structure to those synthesized. Polymers **P2** and **P4** were simulated with the structures given above. For **P1**, the hydrophobic pendant group was changed from $-\text{C}_8\text{H}_{17}$ to $-\text{C}_9\text{H}_{20}$, while for **P3** the hydrophobic pendant simulated was $-\text{C}_3\text{H}_7$ instead of $-\text{C}_2\text{H}_5$. However, polymer **P5**, which has a cyclohexyl pendant group, cannot currently be represented using the SDK force field and hence was omitted from the simulation study.

Single chains were minimized in vacuum, and the resulting structure was replicated and placed randomly on the surface of a sphere such that the hydrophobic groups form the core. One hundred chains were used for each micelle, and the structure was then solvated using CG water and relaxed for ~ 10 ns with a cavitation potential acting on water to stabilize the micelle during equilibration. Subsequently, the cavitation potential was released, and the micelle was equilibrated for a further 20 ns prior to data collection. Coordinates of all beads (including water) were written every 50 ps, while the solute coordinates were written every 10 ps.

Simulations were run for at least 50 ns in the case of micelles absent of drug analogues. For the simulation of drug loaded micelles, micelles were created around a spherical globule of 725 phenol molecules, and simulations were carried out for ~ 100 ns to track the escape of phenol from within the core region to the solvent.

Calculation of Bead Distributions. For each frame of the solute trajectories, the center-of-mass (COM) location of the core is calculated. The distance of each hydrophobic bead and hydrophilic bead from the core COM is tabulated into a histogram with a bin width of 0.1 Å. The final normalized histograms are presented as

Table 1. Molecular Characteristics for Polymers P1–P5^a

polymer	MEEE _m /(M1–M5) _n		M _n ^a (g/mol)(NMR)	M _n ^b (g/mol)(SEC)	PDI
	feed (m:n)	expt (m:n)			
P1	50:50	54:53	27 840	10 540	1.81
P2	50:50	48:46	24 490	10 330	1.61
P3	50:50	47:48	20 660	8 870	1.85
P4	50:50	50:52	25 350	10 850	1.77
P5	50:50	53:56	27 390	10 510	2.02

^aObtained from ¹H NMR analysis by multiplying the degree of polymerization (DP) of the block copolymer with the molecular weight of the monomer repeating unit (DP was estimated from the integration of the methylene benzyl protons vs the methylene protons adjacent to the oxygen in the polymer backbone); *m* indicates the DP of the hydrophilic block, and *n* indicates the DP of the hydrophobic block.

probabilities $P(r)$ as a function of radial distance *r*. The same analysis is carried out for phenol molecules in the case of the drug loaded micelles.

Calculation of Void Volume Fraction. For each frame of the trajectory, 1000 random placed probe points were sampled from within the core of the micelle, and the number of points that did not contact any CG bead were noted. A probe point was considered to be in contact if the distance between the point and the closest bead was smaller than the sum of the probe radius and that bead's van der Waals radius. The fraction of probe points within free volume to the total number of probe points is taken as the void volume. This procedure was repeated for probe radii from 0.0 to 4.0 Å.

Analysis of the Retention of Drug Analogue. The number of drug molecules within 5.0 Å of any hydrophobic pendent bead was recorded as a function of time. This analysis was found to effectively represent the total number of hydrophobic molecules within the core of the micelle. The ability of micelles to retain drug molecules is related to the drug loading capacity.

RESULTS AND DISCUSSION

Synthesis and Characterization of Diblock Copolymer with Different Side Chains. Syntheses of amphiphilic diblock copolymers were performed by sequential monomer addition (Scheme 1). γ -2-[2-(2-Methoxyethoxy)ethoxy]ethoxy- ϵ -caprolactone (MEEE-CL) was used as the hydrophilic monomer, while γ -octyloxy- ϵ -caprolactone (M1), γ -(2-ethylhexyloxy)- ϵ -caprolactone (M2), γ -ethoxy- ϵ -caprolactone (M3), γ -benzyloxy- ϵ -caprolactone (M4), and γ -cyclohexylmethoxy- ϵ -caprolactone (M5) were used as hydrophobic monomers. The polymerizations were performed in bulk at 110 °C at a feeding ratio of MEEE-CL to alkoxy-CL to catalyst to initiator of 50:50:1:1 to ensure that all resulting polymers have comparable composition. Sn(Oct)₂ was used as catalyst, and benzyl alcohol was used as initiator for the ROP of MEEE-CL monomer to generate poly{ γ -2-[2-(2-methoxyethoxy)ethoxy]ethoxy- ϵ -caprolactone}. The sequential addition of γ -alkoxy- ϵ -caprolactone monomer generated the amphiphilic diblock copolymers (Table 1).

Preparation and Characterization of Blank and DOX-Loaded Micelles. Amphiphilic block copolymers self-assemble in aqueous media into micelles whose morphology is dependent on the solvent, molecular weight, and composition of the constituent blocks.³⁵ Our previous study showed that synthesized polymers with similar structure and composition could be assembled into spherical micelles.³⁶ To study the substituent effect on the self-assembled micelles, dynamic light scattering (DLS) and transmission electron microscopy (TEM) were employed to investigate the size and morphology of the resulting micelles. All these diblock copolymers were shown to self-assemble into spherical micelles in aqueous solution as predicted. A typical TEM image of air-dried micelles made from

P1 without any encapsulation is shown in Figure 1B. The image indicates that micelles are well-dispersed, and no apparent

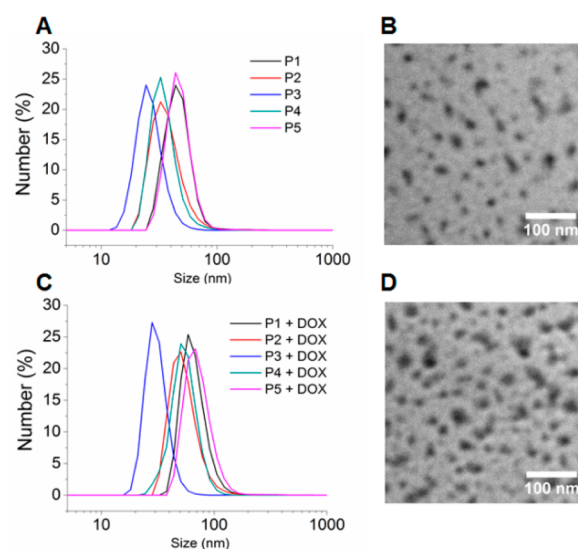


Figure 1. Size distribution of polymeric micelles P1–P5 and TEM images of polymeric micelle P1 before (A, B) and after DOX loading (C, D).

aggregation was observed. The estimated size of the micelles from TEM is ~30 nm. Diblock copolymers P2, P3, P4, and P5 were also observed to form spherical micelles (data not shown). The hydrodynamic volume and zeta potential of all micelles were determined by DLS analysis. As shown in Figure 1A and Table 2, the size of micelles was on the order of tens of nanometers. P1 and P5 micelles had the largest hydrodynamic size, most likely due to the bulky substituents which could result in an increase of the volume of the hydrophobic core. The polydispersity index (PDI) of these two polymeric micelles was also higher, suggesting that the large substituent may contribute to a broadened distribution. Micelles of P3 were found to be the smallest in average size, which could be attributed to the small ethoxy substituent.²⁶ P2 and P4 micelle sizes are in the intermediate range which was not expected, as the branched substituents were expected to create more free volume and give larger micelles.

The hydrophobic core of micelles can sequester and solubilize hydrophobic therapeutic or imaging agents, thus changing the pharmacokinetics and bioavailability.³⁷ Doxorubicin (DOX) was used as a model drug to study the drug loading of the amphiphilic diblock copolymer series. As shown in Figure 1D, the spherical morphology was preserved after

Table 2. Physicochemical Properties of Blank and DOX-Loaded Polymeric Micelles Based on Polymers P1–P5

polymer	CMC (g/L)	LCST (°C)	size (nm)	PDI	zeta potential (mV)	DLC (wt %)	DLC (mol %)	LE (wt %)
P1	6.04×10^{-3}	37.8	45.0 ± 9.1	0.33	-11.3 ± 0.6	NA	NA	NA
P2	4.84×10^{-3}	37.5	37.3 ± 7.4	0.26	-13.6 ± 0.5	NA	NA	NA
P3	8.95×10^{-3}	36.2	26.7 ± 2.4	0.17	-16.2 ± 0.5	NA	NA	NA
P4	2.48×10^{-3}	37.2	35.4 ± 4.0	0.24	-11.9 ± 0.4	NA	NA	NA
P5	1.92×10^{-3}	39.4	47.6 ± 5.8	0.38	-14.8 ± 0.7	NA	NA	NA
P1 + DOX			49.7 ± 17.6	0.42	-12.0 ± 0.1	2.47	63.3	24.7
P2 + DOX			49.2 ± 8.5	0.27	-13.3 ± 0.3	1.59	35.8	15.9
P3 + DOX			31.2 ± 2.5	0.51	-15.4 ± 0.5	2.05	39.0	20.5
P4 + DOX			50.2 ± 10.8	0.46	-12.7 ± 0.6	2.35	54.8	23.5
P5 + DOX			53.1 ± 15.5	0.47	-16.0 ± 0.3	1.41	35.5	14.1

drug loading, and this behavior was observed for all other investigated diblock copolymers (data not shown).

The size of the micelles increased after DOX loading as demonstrated by the DLS analysis shown in Figure 1C and Table 2. This is consistent with what has been observed from previous studies.^{26,38} In addition, all the micelles showed negative surface charge which is desirable because it can prevent dissociation of the micelles caused by serum protein adsorption while being administered in blood plasma.

The drug loading content (DLC) and drug loading efficiency (DLE) were determined by UV–vis spectroscopy. As can be seen from Table 2, the weight percent DLC are relatively low for all five diblock copolymers. However, trends can be estimated based on mole percent DLC. Copolymers P1 and P4 have higher drug content than P2, P3, and P5. For polymer P4, the enhanced π – π interaction between the polymer and DOX molecules could account for the increased DLC. However, despite P1 and P2 having the same number of carbons and similar hydrophobicity, polymer P1 with the linear alkyl substituent had a higher drug loading capacity than P2 with a branched alkyl substituent.

Thermal-Responsive Behavior of the Micelles. The phase transition of diblock copolymers P1–P5 in aqueous solution is attributed to a change in the hydrophilic/hydrophobic equilibrium of the polymers with respect to their interaction through hydrogen bonding between the polymer and water molecules.

LCST was determined by measuring the transmittance of aqueous micellar solutions upon heating. All five amphiphilic diblock copolymers exhibited LCSTs in the range of 36–39 °C. (Figure 2 and Table 2) We have demonstrated in our previous paper that the homopolymer PMEEE had a LCST of 47 °C, while incorporating a hydrophobic block the LCST was decreased to 37 °C.¹⁴ A similar effect was observed for polymers P1–P5, and these polymers had a different thermo-transition range upon heating. Among all polymers, P3 had the

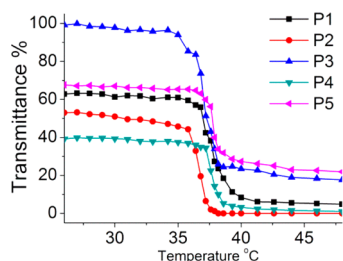


Figure 2. Temperature dependence of transmittance of P1–P5 block copolymers in aqueous solution (0.2 wt % polymer concentration).

largest transmittance drop from 100% to 16%, which is similar to the thermo-transition behavior of PMEEE homopolymer. This is also due to the ethoxy substitution of the core segment which has the highest hydrophilicity among the polymers. The half-transmittance drop point for each polymer was taken as the LCST. It has been observed that LCST is dependent on molecular weight, and a lower LCST was observed for oligo(ethylene glycol)-substituted polymers with a lower molecular weight.³⁹ Even though the LCST is largely dependent on the balance of hydrophobic/hydrophilic blocks, it can be assumed that the differences among the LCST values of the polymers could be attributed to a combination of the hydrophobicity of the core-segment block and the molecular weights.

Substituent Effect on Thermodynamic and Kinetic Stability. The thermodynamic stability is indicated by the critical micellar concentration (CMC) which can be used to estimate the potential of micelles to disassemble. Lower CMC values indicate a higher thermodynamic stability of the micelles. The CMC of micelles was quantified using pyrene as a fluorescent probe. The peak shifted from 335 to 339 nm upon the excitation of pyrene which indicates the incorporation of hydrophobic pyrene molecules in the micelles. The intensity ratio (I_{339}/I_{335}) was plotted against the logarithm of polymer concentration to estimate the CMC value (Figure 3). While the

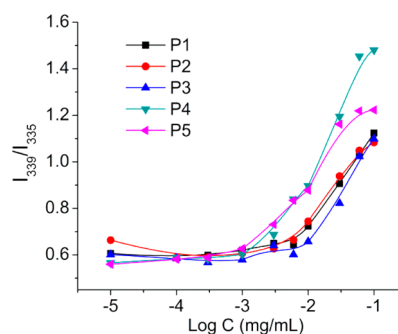


Figure 3. Dependence of intensity ratio I_{339}/I_{335} (from pyrene excitation spectra) as a function of polymer concentration for P1–P5. [Py] = 3.3×10^{-6} M, λ_{em} = 390 nm.

CMC values (Table 2) of these polymers are on the same order of magnitude (10^{-3} mg/mL) they displayed a variation as a function of hydrophobic substituent. Micelles of P3, which have ethoxy substituents on the hydrophobic block, exhibited the highest CMC value. It can be observed that all polymers with branched substituents have lower CMCs than the linear substituents which could be due to the enhanced hydrophobic

interactions among the branched side chains. The decrease in CMC for polymer P4 with benzyloxy functional groups can also be due to increased π - π interactions between polymer chains in the core.⁴⁰ The result suggests that not only the length of hydrophobic segment and hydrophobicity of the backbone polymer^{26,41} but also the physical properties of the substituent on the core-forming segment influence the thermodynamic stability of the micelles. More hydrophobic substituents lead to an increase in both intermolecular and intramolecular hydrophobic-hydrophobic interactions, making the core more rigid upon dilution after administration.

In addition to the thermodynamic stability, Förster resonance energy transfer (FRET) efficiency between FRET pair molecules (DiO/DiI) is used to estimate the kinetic stability, which correlates to the micelle dissociation rate.²⁴ In the initial micelle, both FRET donors and acceptors are encapsulated inside the micelle core and stay in close proximity; thus, the efficiency of FRET should be high. However, if the micelles start to disassemble, donors and acceptors will be released and then diffuse further apart which will decrease the FRET efficiency between the FRET pairs. To test the stability of micelles with different hydrophobic substituents in the core, the FRET pair loaded micelles with equal concentrations were treated with 30% fetal bovine serum (FBS) under mild agitation. The time-resolved fluorescence emission spectra (excitation: 484 nm) of the micelle were recorded at certain time intervals. As shown in Figure 4 (top), increase of DiI signal and quenching of DiO signal were observed for all micelles, indicating the successful formation of micelles and entrapment of FRET pairs. While incubating in FBS containing buffer, the decrease in DiI signal and the increase in DiO signal were observed to different extents which is due to the disruption of micelles by serum proteins and the subsequent

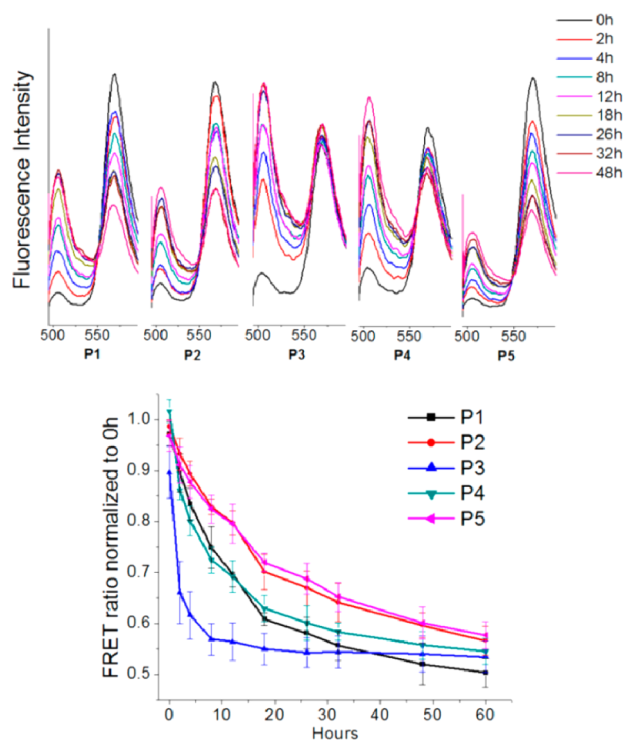


Figure 4. Time-resolved fluorescence spectra of FRET pairs (DiI and DiO) encapsulated in P1–P5 micelles (top). Stability of FRET micelles (P1–P5) in the presence of 30% FBS (bottom).

release of the two dyes. The FRET ratio $I_{565}/(I_{501} + I_{565})$, where I_{501} is the emission intensity of DiO and I_{565} is the emission intensity of DiI, was used to quantify the extent and rate of dissociation. A faster decrease in the FRET ratio also indicates faster dissociation of micelles. For each of polymer micelles, the FRET ratios were normalized to the ratio at time zero and plotted against incubation time, as shown in Figure 4 (bottom). The results imply that micelles of P3 showed the fastest decrease of FRET ratio and reached a plateau only after ~ 10 h of incubation, which indicates that it is the most unstable micelle against serum protein. Micelles composed of P2 and P5 exhibited the slowest FRET ratio decrease and reached a plateau after 60 h, suggesting that the substituents on P2 and P5 help stabilize the micelle and result in higher kinetic stability. The substituents on P1 and P4 have an intermediate stabilizing effect based on the intermediate decrease in FRET ratio.

Substituent Effect on Thermal-Induced Release of Cargo. Thermoresponsivity is one of the most used stimuli that have been employed to achieve stimuli-responsive properties of biomaterials. Thermoresponsive polymer based nanocarriers for drug delivery aim to program temporal drug release in response to the temperature change in the microenvironment. Here we examined the impact of different substituents on the drug release profile in response to an elevation of the local temperature. Nile Red fluorescent probe was encapsulated in the polymeric micelles to estimate the drug release profile. Nile Red is known to have minimal fluorescence in an aqueous environment, whereas its fluorescence increases in a hydrophobic microenvironment such as the micelle core.⁴² Micelles with encapsulated Nile Red were incubated either at elevated temperature (43 °C) (above LCST) or at room temperature (below LCST). The emission spectra (excitation at 570 nm) were recorded at various time intervals. The fluorescence intensity at 620 nm at each time interval was normalized to time zero which was used to represent the release percentage of Nile Red.

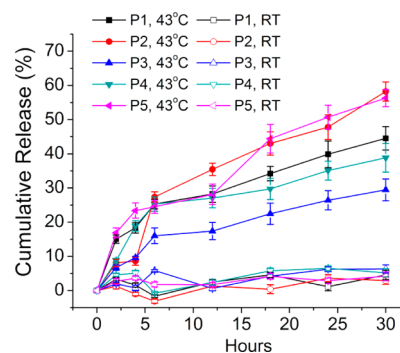


Figure 5. Cumulative Nile Red release from P1–P5 micelles at room temperature (below LCST) and 43 °C (above LCST) in PBS. All measurements were performed in triplicate.

As shown in Figure 5, all micelles showed considerable increase of Nile Red release at 43 °C (higher than the LCST of polymers) when compared to micelles incubated at room temperature (lower than the LCST of polymers), suggesting that the deformation of the hydrophilic outer shell resulted in the release of loaded cargo. Moreover, these micelles with different substituents show different release rates of Nile Red. Nile Red in P2 and P5 micelles exhibited fastest release,

possibly due to the molecular motion of their bulky substituents in the amorphous core which then excluded the cargo from the core. In comparison, the release rate from the **P1** micelle with a linear alkoxy substituent was not as efficient as the **P2** micelle with a branched alkoxy substituent. Additionally, due to the enhanced interaction between the benzyl group on **P4** and Nile Red, the release of Nile Red was diminished. The ethoxy group on **P3** was found to lead to the slowest release of Nile Red from the core. These results suggested that substituents on the core-forming segment do play a role in regulating the release of cargo in addition to the physical properties of the polymer backbone. For **P2** and **P5**, we assumed that molecular motion of bulky substituents expedites the diffusion of the cargo out of the collapsed micelle under elevated temperature, while smaller substituents lead to a slower release of cargo due to a less crowded core. These results shed more light on the rational engineering of the micelle core to achieve programmable release.

Molecular Dynamics Simulations Relating to Micelle Size, Free Volume, and Drug Loading Capacity.

Molecular dynamics simulations were used to gain insight into the behavior and interaction of polymers and drugs. A coarse-grained representation was used for efficiency (Figure 6). Four polymers (**P1–P4**) were modeled resembling the

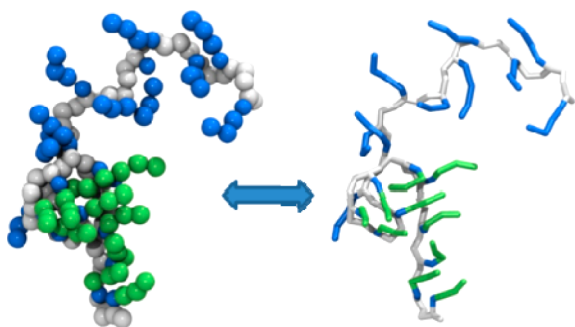


Figure 6. Coarse-grained molecular representation used to model polymers. The beads are colored such that white represents backbone beads, green represents hydrophobic beads, and blue represent hydrophilic beads. Left and right images represent the van der Waals and stick representations for polymer **P1**, respectively.

experimentally studied species. The modeled hydrophobic substituents represent the change in hydrophobic chain length: linear chain vs branched chain and aromatic chain vs nonaromatic chain. All four modeled diblock copolymers formed stable spherical micelles in molecular dynamics simulations with the expected structure of a compact hydrophobic core and a swollen hydrophilic corona (Figure 7).

The **P3** micelle showed the most ellipticity, as it can be observed from Figure 7. This effect was attributed to the size mismatch between the hydrophilic and hydrophobic blocks, leading to the core deforming from a spherical shape with increased surface area. The sizes of the simulated micelles (Figure 8) are smaller than the experimental values which is due to the polymer chain length used in simulations (20 repeat units vs ~ 50 for the synthesized polymers) and the number of chains within a micelle (100 chains/micelle). Furthermore, in experiments polymer chains within a micelle are in dynamic equilibrium with chains in solution, and chains can migrate between micelles until an equilibrium distribution is achieved. In the case of simulations, the number of chains for each

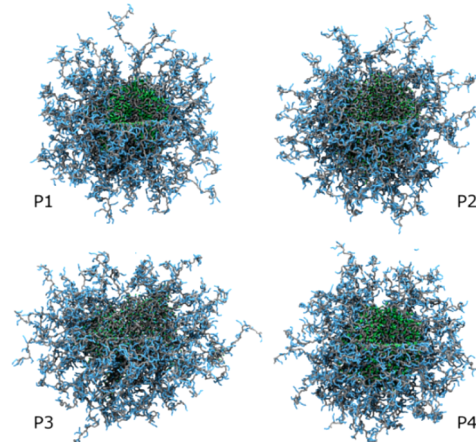


Figure 7. Micelles of polymers **P1–P4** after 50 ns of simulation. Each micelle is a 100 chain aggregate of $A_{20}B_{20}$ -type polymers. Cutouts are used to show the internal structure of the micelles. Coloring as in Figure 6.

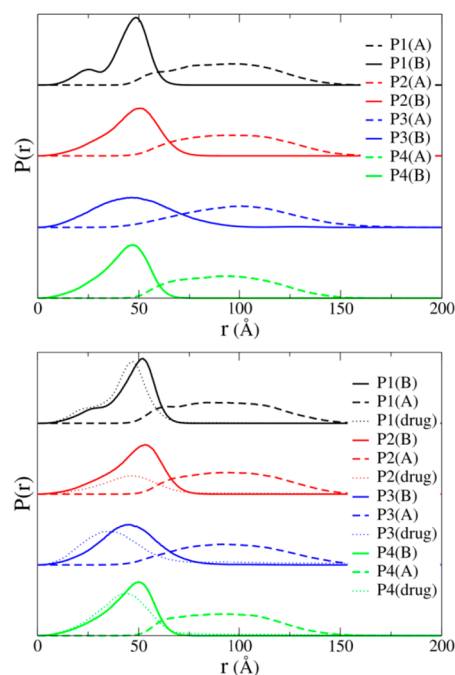


Figure 8. Plots of distance distribution of hydrophilic beads (A) (shown in dashed lines) and hydrophobic beads (B) (shown in solid lines) from the center of simulated micelle cores. The upper plot shows the distribution for the pristine micelles while the lower plot shows those for phenol (listed as drug in the plots) loaded micelles.

micelle remains unchanged. Even with the differences in micelle size between experimental and computational studies, we expect the trends in structural properties and behavior of the micelles to follow the real systems.

Bead Distributions. The distance distribution plots for the investigated diblock copolymer structures are given in Figure 8 for both drug-loaded and unloaded micelles. The comparison of distributions shows only slight changes in the core size and the overall size of the micelles.

For unloaded micelles, the **P3** micelle has the broadest distribution, while micelles of **P1** and **P4** are relatively compact. This may be a result of the shape anisotropy of the micelle of polymer **P3**. The overall micelle size from DLS measurements

are related to the hydrodynamic radius of the micelles, which reflect the hydrophilic corona. The trends shown in simulations are not consistent with the DLS measurements, which could be attributed to the constraint of having a fixed number of chains within a simulated micelle. Moreover, both experimental data and simulation data indicate small variations in the micelle size for polymers **P1–P4**.

Void Volume Measurements. The void volume of the polymer micelles was expected to have implications in predicting the drug loading capacity because the void volume fraction was thought to be indicative of the space available to accommodate the hydrophobic drug molecules. The void volume was analyzed for diblock copolymers **P1–P4** for a range of probe sizes (see Figure 9). The plots follow an

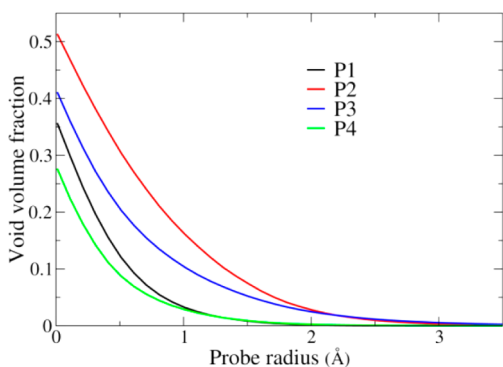


Figure 9. Void volume fraction for polymeric micelles as a function of probe size.

intuitive trend, namely, micelles from diblock copolymers with branched hydrophobic substituent are the least well-packed and consequently have the highest void volume fraction. By contrast, the micelles with linear and benzyl substituents showed better packing, with the benzyl chains showing slightly better packing than the linear alkyl chains (Figure 9).

Drug Loading and Retention. The prediction of drug loading using only void volume neglects two essential factors: (1) the interactions between the drug molecules and polymers and (2) the rearrangement of the polymer chains upon drug loading. We therefore introduced a DOX analogue to better estimate the drug loading capacity. Micelles were created with a high $\sim 10\%$ w/w loading of hydrophobic phenol molecules (Figure 10). Phenol was chosen as the DOX analogue due to its similar octanol:water partitioning behavior. Simulations were run by initially creating a micelle structure around a globule of phenol. Because the number of phenol molecules loaded is initially too high for the core to retain, and due to the partial solubility of phenol in water, some molecules of phenol diffused from the core to the solvent. By tracking the number of phenol molecules retained inside the core, we were able to estimate the drug loading capacity of the polymer micelles. The plot of phenol retention vs time showed the decrease in drug retention within the simulation time frame of 100 ns (Figure 11). This data allows us to estimate the relative drug loading capacity of the micelles as $P3 \sim P2 < P4 < P1$ (Figure 11). This is an important result because the trend shown here is different from what we expected from the void volume measurements which indicated that polymers with branched chains would have the highest loading capacity. However, the simulations for drug loaded micelles show that the branched and short chain groups are the least effective at retaining the drug molecules, which is

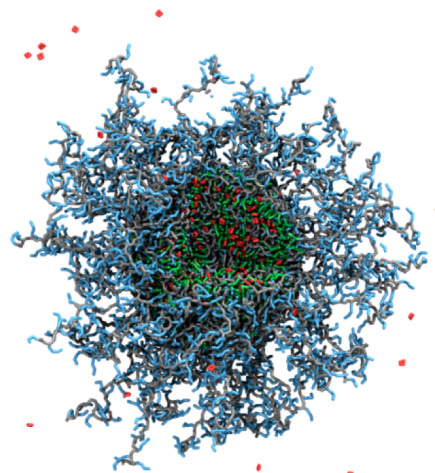


Figure 10. Polymer micelle **P1** loaded with phenol (colored red), the DOX analogue. A cutout is used to show the internal structure of the micelle.

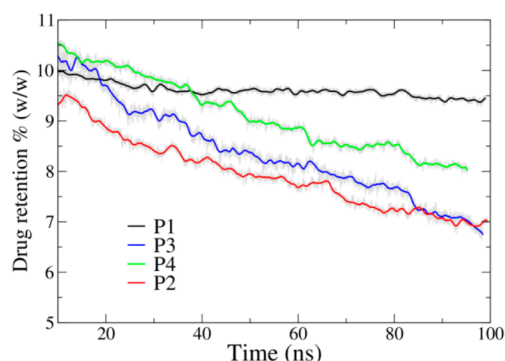


Figure 11. Prediction of drug loading capacity on $A_{20}B_{20}$ -type polymers by using nondegenerative drug (diffusion) release.

possibly due to the inefficient packing of the phenol molecules with the core substituents and weak interactions between the drug analogue and the polymer chains. The benzyl and octyl groups have a high loading; π - π interactions may be partly responsible for the better performance of the aromatic group.

This trend of drug loading behavior was further supported by the probability bead distributions (Figure 8). Based on the overlapping intensity and areas of the phenol molecule distribution with the hydrophobic block distribution, a similar trend of $P3 < P2 < P4 < P1$ can be estimated. Note that the number of drug molecules found between r and $r + dr$ from the micelle core center is $4\pi r^2 P(r) dr$, so that a drug distribution peaked at a larger r value contains many more drug molecules.

Overall, the molecular dynamics simulation data agreed with the experimental findings that the straight linear chain octyloxy and the aromatic benzyloxy offer the best drug loading capacity. The analysis of void volume does not follow this trend, indicating that the interactions of the drug with the polymers play an important role in the loading of drugs into these block copolymer micelles.

Thermal Analysis. The glass transition temperatures (T_g) of the polymers **P1–P5** were determined by DSC analysis (Table 3 and Supporting Information). All the copolymers displayed two T_g values corresponding to each block. The T_g for the common hydrophilic poly[γ -2-[2-(2-methoxyethoxy)ethoxy]-ethoxy- ϵ -caprolactone] block was -82 °C for all the diblock

Table 3. Glass Transition Temperatures of the Diblock Copolymers P1–P5^a

polymer	T_g^1 (°C)	T_g^2 (°C)	polymer	T_g^1 (°C)	T_g^2 (°C)
P1	-82	-70	P4	-82	-51
P2	-82	-68	P5	-82	-63
P3	-82	-64			

^a T_g^1 = glass transition temperature of the hydrophilic block; T_g^2 = glass transition temperature of the hydrophobic block.

copolymers. Considering the second T_g for the diblock copolymers P1–P5, which corresponds to the hydrophobic block, the polymer P4 containing poly(γ -benzyloxy- ϵ -caprolactone) had the highest T_g of -51 °C, which is due to the presence of the bulky phenyloxy group. By contrast, the diblock copolymer P1 containing the hydrophobic poly(γ -octyloxy- ϵ -caprolactone) had the lowest T_g of -70 °C which was attributed to the relatively flexible octyloxy substituents. No melting temperature transitions were detected on the DSC thermograms which confirmed the amorphous nature of copolymers P1–P5.

CONCLUSION

Five γ -substituted caprolactone hydrophobic monomers were synthesized and used to generate amphiphilic thermosensitive polycaprolactone diblock copolymers. The five polymers (P1–P5) were synthesized by ring-opening polymerization with Sn(Oct)₂ catalyst. The synthesized amphiphilic diblock copolymers formed micelles in an aqueous environment and maintained the thermoresponsive behavior imparted by the PEEEE block. The synthesized micelles were found to be thermodynamically and kinetically stable and showed thermocontrolled release behavior upon temperature increase above LCST. The drug loading capacity (DLC) of the micelles were estimated to probe the difference generated by the variation of the substituents on the hydrophobic block. The DLC was estimated both experimentally by using UV–vis spectroscopy and computationally (using phenol as the DOX analogue) by molecular dynamics modeling. Molecular dynamics simulations showed a similar trend in DLC based on the substituent change as the experiments. These findings are expected to provide an easy computational method to predict drug loading before the synthesis of amphiphilic diblock copolymers and could become a valuable tool for the engineering of micellar drug delivery systems.

ASSOCIATED CONTENT

Supporting Information

Experimental procedures for the synthesis of caprolactone monomers, ¹H and ¹³C NMR spectra. This material is available free of charge via the Internet at <http://pubs.acs.org>.

AUTHOR INFORMATION

Corresponding Author

*E-mail: mci071000@utdallas.edu (M.C.S.).

Author Contributions

§J.H. and Y.C. contributed equally.

Notes

The authors declare no competing financial interest.

ACKNOWLEDGMENTS

Steven O. Nielsen and Udayana Ranatunga thank Dr. Sharon Loverde for her assistance and also acknowledge Texas Advanced Computing Center (TACC) at The University of Texas at Austin for providing HPC resources that have contributed to the research results reported within this paper. Mihaela C. Stefan acknowledges financial support from NSF (DMR-0956116 and CHE-1126177) and Welch Foundation (AT-1740). Qian Wang acknowledges the financial support from NSF CAREER CHE-0748690 and the Camille Dreyfus Teacher Scholar Award.

REFERENCES

- Rosler, A.; Vandermeulen, G. W. M.; Klok, H.-A. *Adv. Drug Delivery Rev.* **2012**, *64* (Suppl.), 270–279.
- Kataoka, K.; Harada, A.; Nagasaki, Y. *Adv. Drug Delivery Rev.* **2012**, *64* (Suppl.), 37–48.
- Tyrrell, Z. L.; Shen, Y.; Radosz, M. *Prog. Polym. Sci.* **2010**, *35*, 1128–1143.
- Gaucher, G.; Dufresne, M.-H.; Sant, V. P.; Kang, N.; Maysinger, D.; Leroux, J.-C. *J. Controlled Release* **2005**, *109*, 169–188.
- Abetz, V.; Gohy, J.-F. In *Block Copolymers II*; Springer: Berlin, 2005; Vol. 190, pp 65–136.
- Jérôme, C.; Lecomte, P. *Adv. Drug Delivery Rev.* **2008**, *60*, 1056–1076.
- Philippe, L.; Raphaël, R.; Stéphanie, S.; Jutta, R.; Kathy Van, B.; Christine, J.; Robert, J. *Macromol. Symp.* **2006**, *240*, 157–165.
- Albertsson, A.-C.; Varma, I. K. *Biomacromolecules* **2003**, *4*, 1466–1486.
- Xiong, X.-B.; Falamarzian, A.; Garg, S. M.; Lavasanifar, A. *J. Controlled Release* **2011**, *155*, 248–261.
- Xiong, X.-B.; Ma, Z.; Lai, R.; Lavasanifar, A. *Biomaterials* **2010**, *31*, 757–768.
- Xiong, X.-B.; Uludağ, H.; Lavasanifar, A. *Biomaterials* **2009**, *30*, 242–253.
- Yang, C.; Ebrahim Attia, A. B.; Tan, J. P. K.; Ke, X.; Gao, S.; Hedrick, J. L.; Yang, Y.-Y. *Biomaterials* **2012**, *33*, 2971–2979.
- Garg, S. M.; Xiong, X.-B.; Lu, C.; Lavasanifar, A. *Macromolecules* **2011**, *44*, 2058–2066.
- Hao, J.; Servello, J.; Sista, P.; Biewer, M. C.; Stefan, M. C. *J. Mater. Chem.* **2011**, *21*, 10623–10628.
- Su, R.-J.; Yang, H.-W.; Leu, Y.-L.; Hua, M.-Y.; Lee, R.-S. *React. Funct. Polym.* **2012**, *72*, 36–44.
- Dai, W.; Huang, H.; Du, Z.; Lang, M. *Polym. Degrad. Stab.* **2008**, *93*, 2089–2095.
- Darcos, V.; El Habnoui, S.; Nottelet, B.; El Ghzaoui, A.; Coudane, J. *Polym. Chem.* **2010**, *1*, 280–282.
- Ward, M. A.; Georgiou, T. K. *Polymers* **2012**, *3*, 1215–1242.
- Bajpai, A. K.; Shukla, S. K.; Bhanu, S.; Kankane, S. *Prog. Polym. Sci.* **2008**, *33*, 1088–1118.
- Ganta, S.; Devalapally, H.; Shahiwala, A.; Amiji, M. *J. Controlled Release* **2008**, *126*, 187–204.
- Lutz, J.-F.; Akdemir, Ö.; Hoth, A. *J. Am. Chem. Soc.* **2006**, *128*, 13046–13047.
- Lutz, J.-F.; Hoth, A. *Macromolecules* **2005**, *39*, 893–896.
- Kim, S. H.; Tan, J. P. K.; Fukushima, K.; Nederberg, F.; Yang, Y. Y.; Waymouth, R. M.; Hedrick, J. L. *Biomaterials* **2011**, *32*, 5505–5514.
- Cheng, Y.; Hao, J.; Lee, L. A.; Biewer, M. C.; Wang, Q.; Stefan, M. C. *Biomacromolecules* **2012**, *13*, 2163–2173.
- Mahmud, A.; Patel, S.; Molavi, O.; Choi, P.; Samuel, J.; Lavasanifar, A. *Biomacromolecules* **2009**, *10*, 471–478.
- Zhao, X.; Poon, Z.; Engler, A. C.; Bonner, D. K.; Hammond, P. T. *Biomacromolecules* **2012**, *13*, 1315–1322.
- Patel, S. K.; Lavasanifar, A.; Choi, P. *Biomaterials* **2010**, *31*, 1780–1786.

- (28) Patel, S. K.; Lavasanifar, A.; Choi, P. *Biomaterials* **2010**, *31*, 345–357.
- (29) Lu, J.; Owen, S. C.; Shoichet, M. S. *Macromolecules* **2011**, *44*, 6002–6008.
- (30) Shinoda, W.; DeVane, R.; Klein, M. L. *Mol. Simul.* **2007**, *33*, 27–36.
- (31) Shinoda, W.; DeVane, R.; Klein, M. L. *Soft Matter* **2008**, *4*, 2454–2462.
- (32) Loverde, S. M.; Klein, M. L.; Discher, D. E. *Adv. Mater.* **2011**, *24*, 3823–3830.
- (33) Plimpton, S. J. *Comput. Phys.* **1995**, *117*, 1–19.
- (34) Shinoda, W.; Shiga, M.; Mikami, M. *Phys. Rev. B* **2004**, *69*, 134103.
- (35) Kim, J. K.; Yang, S. Y.; Lee, Y.; Kim, Y. *Prog. Polym. Sci.* **2010**, *35*, 1325–1349.
- (36) Cheng, Y.; Hao, J.; Lee, L. A.; Biewer, M. C.; Wang, Q.; Stefan, M. C. *Biomacromolecules* **2012**, *13*, 2163–2173.
- (37) Kataoka, K.; Harada, A.; Nagasaki, Y. *Adv. Drug Delivery Rev.*
- (38) Yan, J.; Ye, Z.; Chen, M.; Liu, Z.; Xiao, Y.; Zhang, Y.; Zhou, Y.; Tan, W.; Lang, M. *Biomacromolecules* **2011**, *12*, 2562–2572.
- (39) Han, S.; Hagiwara, M.; Ishizone, T. *Macromolecules* **2003**, *36*, 8312–8319.
- (40) Carstens, M. G.; Bevernage, J. J. L.; van Nostrum, C. F.; van Steenberghe, M. J.; Flesch, F. M.; Verrijck, R.; de Leede, L. G. J.; Crommelin, D. J. A.; Hennink, W. E. *Macromolecules* **2006**, *40*, 116–122.
- (41) Owen, S. C.; Chan, D. P. Y.; Shoichet, M. S. *Nano Today* **2012**, *7*, 53–65.
- (42) Jackson, A. W.; Fulton, D. A. *Macromolecules* **2012**, *45*, 2699–2708.